International Journal of Pharmacology

Int. J. Pharmacol. **2026**; 22(5): 54359
https://doi.org/10.31083/IJP54359

Research Article

Dose-Dependent Effects of Metformin Preconditioning on Metabolic, Clonogenic, and Differentiation-Associated Responses in Human Umbilical Cord-Derived Mesenchymal Stromal Cells: An Exploratory *In Vitro* Study

Mah Jabeen Muneera[1,*], Muhammad Mustahsan Bashir[2], Nighat Yasmin[3], Muhammad Shakil[4], Aamir Jamal Gondal[3]

[1]Department of Anatomy, Allama Iqbal Medical College, 54550 Lahore, Punjab, Pakistan
[2]Department of Plastic Surgery, King Edward Medical University, 54700 Lahore, Punjab, Pakistan
[3]Advanced Research Centre for Biomedical Sciences, King Edward Medical University, 54700 Lahore, Punjab, Pakistan
[4]Department of Biochemistry, King Edward Medical University, 54700 Lahore, Punjab, Pakistan
*Correspondence: munira.ashfaq@gmail.com (Mah Jabeen Muneera)
Academic Editor: Mehmet Ozaslan
Submitted: 30 May 2026 Revised: 28 July 2026 Accepted: 14 August 2026 Published: 20 September 2026

Abstract

Background: Human umbilical cord-derived mesenchymal stromal cells (UC-MSCs) are used in regenerative research, but culture performance varies across donors. Metformin may modulate cellular metabolism and lineage-associated responses, although its effects are dose- and context-dependent. Therefore, this study aimed to evaluate the effects of metformin on metabolic, clonogenic, expansion, and differentiation responses in UC-MSC cultures. **Methods:** Wharton's jelly cultures were established from individual umbilical cords without pooling. Qualitative immunofluorescence supported a stromal phenotype. 2,3-bis(2-methoxy-4-nitro-5-sulfophenyl)-2H-tetrazolium-5-carboxanilide (XTT) metabolic activity was assessed at 0–1000 µM metformin (n = 10 donors); colony-forming unit–fibroblast (CFU-F)/plating efficiency at 0, 100, 500, and 1000 µM (n = 9); interval population doubling (PD) and descriptive population doubling time (PDT) across P3–P6 (n = 6 complete donors); exploratory osteogenic and neurogenic induction-associated morphology after 100 µM preconditioning (n = 9). Within-donor comparisons used Friedman tests and exact paired Wilcoxon tests with Holm adjustment. **Results:** XTT signal varied across concentrations (χ^2 (6) = 57.88, $p < 0.001$; Kendall's W = 0.965), peaking at a median of 106.39% of control at 100 µM and declining to 95.51% at 1000 µM. CFU-F/plating efficiency also differed (χ^2 (3) = 19.99, $p < 0.001$; W = 0.740): medians were 5.23% in controls, 6.60% at 100 µM (Holm $p = 0.039$), 4.57% at 500 µM ($p = 0.039$), and 3.13% at 1000 µM ($p = 0.035$). PD showed ordered dose patterns at each passage (Holm-adjusted omnibus $p < 0.001$), but no dose-versus-control contrast remained significant after the 12-comparison Holm adjustment. Osteogenic scores did not differ ($p = 0.445$); the neurogenic-associated score was higher after 100 µM ($p = 0.008$) but remained exploratory. **Conclusions:** Metformin was associated with concentration-dependent phenotypic responses in UC-MSCs. The 100 µM condition produced the highest XTT signal and CFU-F/plating efficiency, whereas higher concentrations were associated with lower clonogenic and expansion measures. These findings do not establish mature neuronal differentiation, a molecular mechanism, or therapeutic efficacy and require confirmation in rigorously characterized models.

Keywords: metformin; mesenchymal stromal cells; umbilical cord; Wharton's jelly; population doubling; differentiation-associated morphology

1. Introduction

Human umbilical cord-derived mesenchymal stromal cells (UC-MSCs) are attractive for regenerative research because Wharton's jelly is readily available after delivery and cells can be expanded without an invasive donor procedure [1]. The commonly cited minimum criteria for mesenchymal stromal cells include plastic adherence, a defined surface marker profile, and osteogenic, adipogenic, and chondrogenic differentiation [2]. These criteria do not eliminate donor- and manufacturing-related heterogeneity in clonogenicity, expansion, responsiveness to differentiation, and other functional properties [3,4].

Pharmacological preconditioning aims to modify cellular behavior before a downstream application. Metformin is a mitochondrial and energy-sensing modulator whose effects involve multiple AMP-activated protein kinase (AMPK)-dependent and AMPK-independent processes [5]. Reviews of mesenchymal stromal cells describe dose-, source-, passage-, and exposure-dependent effects on proliferation, senescence, and differentiation [6]. In human UC-MSCs and related perinatal stromal cell models, low-to-intermediate concentrations have been associated with osteogenic responses, whereas higher concentrations can suppress growth [7,8,9,10]. These pathways provide biological context but cannot be attributed to a specific experiment unless they are directly measured.

Therefore, the concentration–response relationship is central to any preconditioning strategy. 2,3-bis(2-methoxy-4-nitro-5-sulfophenyl)-2H-tetrazolium-5-carboxanilide (XTT) reduction can identify changes in cellular metabolic activity but does not directly measure cell number, proliferation, apoptosis, or all domains of toxicity. Clonogenic assays and serial expansion provide complementary phenotypic information. Evidence for metformin-associated neural lineage responses is derived mainly from neural stem/progenitor models [11]; findings in UC-MSC cultures based solely on morphology must be described as neurogenic induction-associated responses rather than as mature neuronal conversion.

Few human UC-MSC studies have assessed a range of metformin doses using multiple donor-paired functional endpoints. Thus, this study aimed to evaluate XTT metabolic activity, colony-forming unit–fibroblast (CFU-F) plating efficiency, interval PD and PDT across passages, and exploratory osteogenic- and neurogenic induction-associated morphology in independently maintained donor-derived cultures. The objective was to identify a concentration-associated phenotypic pattern while keeping all conclusions within the limits of the available assays.

2. Materials and Methods

2.1 Study Design and Setting

This comparative exploratory *in vitro* study evaluated untreated and metformin-exposed UC-MSC cultures derived from human Wharton's jelly. Laboratory work was performed at the Advanced Research Centre of Biomedical Sciences, King Edward Medical University, under Biosafety Level 2 conditions.

2.2 Ethical Approval and Consent

The study was approved by the Institutional Ethics Review Committee of King Edward Medical University (No. 1030/RC/KEMU; 21 August 2019) and was conducted in accordance with the Declaration of Helsinki. Umbilical cords were collected after obtaining written informed consent from the mothers following routine delivery, without altering obstetric care. No identifiable maternal or neonatal information was retained.

2.3 Donors, Culture Eligibility, and Statistical Unit

A total of 15 cords were documented. UC01 and UC02 produced no outgrowth. UC10 and UC11 developed visible contamination, morphologically consistent with bacterial contamination. Both cultures were discarded upon detection of contamination and excluded from all inferential analyses. The incubator and biosafety cabinet were decontaminated. A total of 11 cultures were documented as successful outgrowths without overt contamination. Routine culture-quality monitoring consisted of daily visual inspection for morphology, confluence, and overt contamination; no specific mycoplasma detection assay was performed. Cultures from different donors were maintained separately and not pooled. The donor was the biological unit; technical wells, dishes, counts, or microscopic fields were averaged within each donor before inference. Eligibility was assay-specific: XTT used the original set of 10 donors; CFU-F and morphology used 9 donors without recorded overt contamination; longitudinal PD/PDT used 6 donors with complete P3–P6 records.

2.4 Cord Collection, Isolation, and Expansion

A 5–10 cm cord segment was transported in sterile phosphate-buffered saline containing penicillin, streptomycin, and amphotericin B at 4–8 °C and processed within 1–2 hours. After removing the vessels, Wharton's jelly was cut into 2–3 mm^3 explants and seeded into T-25 flasks. Cultures were expanded in alpha-minimum essential medium (α-MEM; Cat. No. 32571036, Gibco, Thermo Fisher Scientific, Paisley, Scotland, UK) supplemented with 10% heat-inactivated fetal bovine serum (FBS; Cat. No. F9665, Sigma-Aldrich, St. Louis, Missouri, USA), L-glutamine/GlutaMAX, penicillin–streptomycin, and non-essential amino acids (NEAA; Cat. No. NAL03, Caisson Labs, Smithfield, Utah, USA) at 37 °C and 5% CO_2. Cells were passaged at 70–80% confluence using 0.25% trypsin–EDTA (Cat. No. TRL01, Caisson Labs, Smithfield, Utah, USA) and counted by 0.4% trypan blue exclusion (Cat. No. 15250061, Gibco, Thermo Fisher Scientific, Grand Island, New York, USA). Experimental assays used early passages, primarily P3–P5.

2.5 Qualitative Immunophenotypic Characterization

Qualitative immunophenotypic characterization was performed on an initial subset of early-passage, primary donor-derived UC-MSC cultures after the isolation protocol was established; the exact number of characterized donor cultures was not recorded. P3–P5 cells were seeded onto sterile glass coverslips in 24-well plates and allowed to attach for 24–48 hours. Cells were washed with phosphate-buffered saline and fixed with 4% paraformaldehyde (Cat. No. P6148, Sigma-Aldrich, St. Louis, Missouri, USA) at room temperature for 15 minutes. Where required, cells were permeabilized with 0.1% Triton X-100 (Cat. No. T8787, Sigma-Aldrich, Milwaukee, Wisconsin, USA) in phosphate-buffered saline for approximately 5 minutes, and non-specific binding was blocked with 1% bovine serum albumin (BSA; Cat. No. 15260037, Gibco, Thermo Fisher Scientific, Grand Island, New York, USA) in phosphate-buffered saline for 30 minutes. Primary monoclonal antibodies included PE-conjugated CD44 (1:200; Cat. No. 12-0441-82, Invitrogen/eBioscience), CD73 (1:100; Cat. No. sc-398260, Santa Cruz Biotechnology), CD90 (1:250; Cat. No. 14-0909-82, Invitrogen/eBioscience), CD105 (1:100; Cat. No. sc-18838, Santa Cruz Biotechnology), CD14 (1:200; Cat. No. 13-0149-82, Invitrogen/eBioscience), CD34 (1:200; Cat. No. sc-7045, Santa Cruz Biotech-

nology), and CD45 (1:200; Cat. No. sc-53045, Santa Cruz Biotechnology). Mouse-derived primary antibodies were detected using a Tetramethylrhodamine isothiocyanate (TRITC)-conjugated anti-mouse secondary antibody (1:200; Cat. No. sc-3796, Santa Cruz Biotechnology), rat-derived primary antibodies with a Fluorescein isothiocyanate (FITC)-conjugated anti-rat secondary antibody (1:200; Cat. No. ab6848-1, Abcam), and nuclei were stained with 4′,6-Diamidino-2-phenylindole (DAPI). Coverslips were mounted with anti-fade medium and examined using an Olympus BX61 epifluorescence microscope equipped with an Olympus DP70 digital camera at a 10× objective. Mouse, rat, unstained, and secondary-only controls were used to assess background and non-specific fluorescence. No flow cytometry, short tandem repeat (STR) profiling, or other independent authentication assay was performed; therefore, the images were treated as qualitative phenotype support rather than quantitative confirmation of International Society for Cellular Therapy (ISCT) thresholds [2].

2.6 Metformin Working Solutions and Exposure Schedule

Metformin hydrochloride (Cat. No. S1950, Selleck Chemicals LLC, Houston, TX, USA) was dissolved in complete culture medium to prepare a sterile 1 mM working treatment solution; lower treatment concentrations were prepared by dilution with complete medium. The available record did not support describing this as a separately concentrated primary stock. XTT conditions were 0, 50, 100, 200, 400, 800, and 1000 µM for 24 hours after a 24-hour attachment period. CFU-F cultures received 0, 100, 500, or 1000 µM during the 10–14-day colony-formation period. The same four conditions were maintained during serial expansion intervals for PD/PDT. Differentiation experiments used 48-hour preconditioning with 100 µM metformin before induction; control cultures received complete medium without metformin.

2.7 XTT Metabolic Activity Assay

Cells were seeded at 1×10^4 cells/well in 96-well plates and allowed to attach for 24 hours. After a 24-hour exposure to control or metformin-containing medium, the XTT reaction mixture was added and incubated for 3–4 hours in the dark. Absorbance was measured at 450 nm with a reference at 640 nm. Cell-free blanks were subtracted, technical replicates were averaged within each donor, and each treated condition was expressed as a percentage of the untreated control for that donor. XTT was interpreted as a measure of metabolic reduction rather than a direct cell count or a comprehensive toxicity assay [12].

2.8 CFU-F and Plating Efficiency

A total of 1000 viable cells were seeded per dish under each condition and cultured for 10–14 days, with the medium renewed every 3–4 days. Cultures were fixed in methanol, stained with 0.5% crystal violet, and colonies containing at least 50 cells were counted. Three dish counts were averaged for each donor–condition. CFU-F/plating efficiency (%) was calculated as mean colonies divided by 1000 seeded cells × 100 [13]. Since the seeding denominator was fixed at 1000, the CFU-F percentage and plating efficiency were treated as a single numerical endpoint.

2.9 Population Doubling and Population Doubling Time

Counts of viable seeded and harvested cells were recorded for P3–P6 at 0, 100, 500, and 1000 µM metformin. Interval PD was recalculated as $\log_2(Nh/Ns)$, where Nh is the harvested viable count and Ns is the seeded count. PDT was calculated as the interval duration in hours divided by the count-derived PD. PDT was not calculated when PD was zero or negative; such observations were reported as no net expansion or net cell loss.

2.10 Osteogenic Induction and Qualitative Mineralization

P3–P5 cultures were seeded at approximately 5×10^3 viable cells/cm^2, assigned to control or 100 µM metformin, and preconditioned for 48 hours. Cultures were then maintained for 14 days in complete StemPro osteogenic differentiation medium, with the medium renewed every 3–4 days. Morphology and modified Von Kossa staining were documented on day 14. Von Kossa deposits were interpreted qualitatively; no optical density or automated image quantification data were available.

2.11 Neurogenic Induction-Associated Morphology

P3–P5 cultures were seeded at approximately 1.5–2.0 $\times 10^4$ cells/cm^2, preconditioned for 48 hours, and then exposed to neurobasal medium supplemented with neural induction supplement on standard culture-treated plates. The medium was renewed every 2–3 days, and morphology was documented on days 7 and 14. Only matched day-14 control and 100 µM metformin images are shown (Fig. 6). The outcome is described as neurogenic induction-associated morphology rather than neuronal differentiation.

2.12 Exploratory Morphology Scores

Three recorded microscopic field scores (1–5) were averaged for each donor–condition. Osteogenic anchors ranged from predominantly spindle-shaped cells with rare deposits (score 1) to extensive coalescent mineral-associated deposits and polygonal/multilayered cells (score 5). Neurogenic anchors ranged from spindle-shaped cells without processes (score 1) to predominantly polarized bipolar or multipolar cells with elongated, branched processes and network-like arrangements (score 5). The original records did not permit verification of observer number, blinding, inter-rater reliability, or a prospectively validated rubric. The neurogenic scores were derived from matched day-14 images. Scores were treated as exploratory ordinal outcomes.

Table 1. Donor-normalized XTT metabolic activity signal by metformin concentration.

Metformin (μM)	n	Median % control [IQR]	HL shift vs. 0 (pp)	Holm *p*
0	10	100.00 [100.00–100.00]	Reference	-
50	10	102.24 [101.92–102.42]	+2.24	0.012
100	10	106.39 [105.51–106.95]	+6.25	0.012
200	10	100.46 [100.40–100.86]	+0.63	0.012
400	10	103.04 [102.40–103.41]	+2.91	0.012
800	10	99.55 [98.72–100.34]	–0.45	0.250
1000	10	95.51 [94.44–96.09]	–4.65	0.012

IQR, interquartile range; HL, Hodges–Lehmann paired shift; pp, percentage points. Holm family size = 6. XTT represents the metabolic reduction relative to the control for each donor.

2.13 Source Data Exclusions

Quantitative PCR findings were excluded from the revised report because the later Ct workbook could not be reconciled with the original instrument export, the documented biological replicate count, the primer order, or the available AriaMx photographs. No qPCR fold change, *p*-value, graph, or confirmatory gene expression statement was reported.

2.14 Statistical Analysis

Continuous endpoints were summarized using the median and interquartile range (IQR). Within-donor omnibus comparisons used Friedman tests with Kendall's W. Prespecified treated-versus-control comparisons used exact two-sided Wilcoxon signed-rank tests obtained by sign enumeration with midranks for ties and zero differences omitted. Effect estimates were reported as Hodges–Lehmann paired shifts. Holm adjustment governed the six XTT, three CFU-F, 12 passage-specific PD, and two morphology contrast families. A Gaussian longitudinal mixed model was attempted for PD, but a variance component collapsed to the boundary, and residuals were heavy-tailed; therefore, the prespecified passage-specific non-parametric fallback governed PD inference. PDT was descriptive. Analyses were two-sided at $\alpha = 0.05$ and were performed in Python 3.12.13 (Python Software Foundation; https://www.python.org/) with pandas 2.2.3 (pandas development team; https://pandas.pydata.org/) and SciPy 1.17.0 (SciPy developers; https://scipy.org/).

3. Results

3.1 Culture Morphology and Qualitative Immunophenotype

Explants produced adherent, spindle-shaped stromal cultures with fibroblast-like, whorl-forming morphology in early passage. Qualitative immunofluorescence images showed staining for CD44, CD73, CD90, and CD105, with minimal staining for CD14, CD34, and CD45. These observations supported a phenotype consistent with UC-MSCs but did not constitute quantitative or complete cell authentication; no marker-positive percentages were obtained (Fig. 1).

3.2 XTT Metabolic Activity Response

Metformin concentration was associated with a consistent within-donor XTT pattern (Friedman χ^2 (6) = 57.88, $p < 0.001$; Kendall's W = 0.965). The median signal was highest at 100 μM (106.39% of donor-specific control) and lowest at 1000 μM (95.51%). Relative to control, the 50, 100, 200, 400, and 1000 μM contrasts remained significant after Holm adjustment (all $p = 0.012$); the 800 μM contrast did not ($p = 0.250$) (Table 1; Fig. 2).

3.3 CFU-F/Plating Efficiency

CFU-F/plating efficiency differed across concentrations (Friedman χ^2 (3) = 19.99, $p < 0.001$; Kendall's W = 0.740). The median was 5.23% in controls and 6.60% at 100 μM (HL shift +1.20 percentage points; Holm $p = 0.039$). Values were lower at 500 μM (4.57%; shift –0.67; $p = 0.039$) and 1000 μM (3.13%; shift –1.90; $p = 0.035$) (Table 2; Fig. 3).

3.4 Interval Population Doubling and Descriptive PDT

The longitudinal mixed model did not pass the prespecified stability check. Under the governing passage-specific fallback, dose distributions differed across P3–P6 (all Holm-adjusted exact omnibus $p < 0.001$; Kendall's W = 0.944 at P3 and 1.000 at P4–P6). Median interval PD was highest at 100 μM from P4 onward and lower at 500 and 1000 μM; however, none of the 12 dose-versus-control contrasts remained significant after family-wise Holm adjustment (all adjusted $p = 0.375$). At P3, one donor in the 1000 μM group showed net cell loss (PD = –0.037), so PDT was not calculable for that interval (Table 3; Fig. 4).

3.5 Exploratory Osteogenic Morphology

Both control and 100 μM metformin cultures showed osteoblast-like morphological changes and mineral-associated deposits on modified Von Kossa staining. These observations were qualitative. The paired field-score median was 2.67 [IQR 2.67–2.67] in controls and 2.67 [2.33–3.33] with 100 μM metformin; the adjusted paired comparison was not significant (HL shift +0.17 points; Holm $p = 0.445$) (Table 4; Fig. 5).

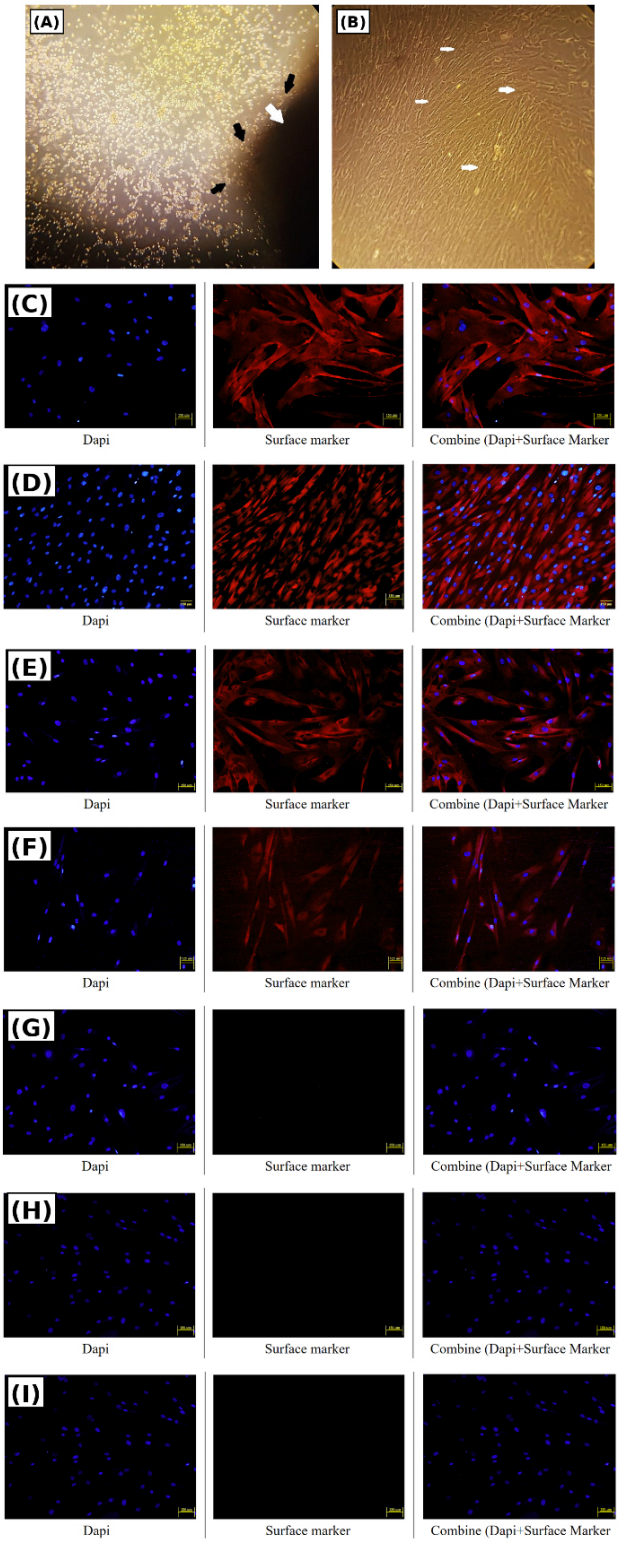

Fig. 1. Representative culture morphology and qualitative immunofluorescence characterization. (A) Explant outgrowth showing the explant edge (white arrow) and early MSCs emerging from it (black arrows). (B) Spindle-shaped stromal cell morphology (white arrows). (C–F) Staining for CD44 (C), CD90 (D), CD105 (E), and CD73 (F). (G–I) Minimal staining for CD34 (G), CD45 (H), and CD14 (I). Each marker row includes DAPI, the corresponding marker channel, and merged views. Images are qualitative; no flow-cytometric percentages were inferred. Immunofluorescence images were recorded at 10× magnification. Scale bars in panels C–I represent 100 μm; panels A and B do not contain scale bars.

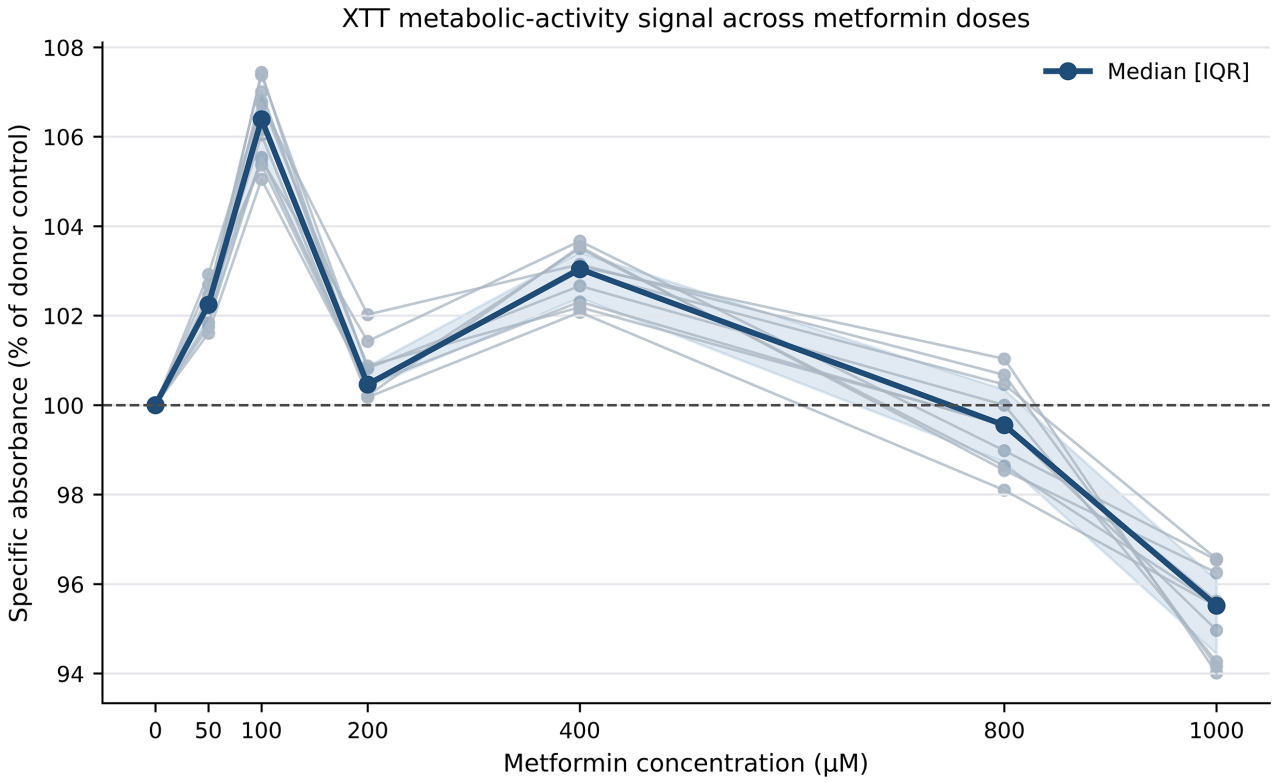

Fig. 2. Donor-specific XTT metabolic activity across metformin concentrations (n = 10). Thin lines show donor trajectories; the heavy line shows the median with IQR. Friedman χ^2 (6) = 57.88, $p < 0.001$; Kendall's W = 0.965. Exact paired Wilcoxon signed-rank control contrasts were adjusted using Holm's method (family size = 6; Table 1).

Table 2. Recalculated CFU-F/plating efficiency results.

Metformin (µM)	n	Median % [IQR]	HL shift vs. 0 (pp)	Holm *p*
0	9	5.23 [4.83–5.70]	Reference	-
100	9	6.60 [6.30–6.90]	+1.20	0.039
500	9	4.57 [4.30–5.43]	–0.67	0.039
1000	9	3.13 [2.83–4.27]	–1.90	0.035

Values were recalculated from three dish counts per donor–condition. Since 1000 cells were seeded, the CFU-F percentage and the plating efficiency percentage are the same endpoint. Holm family size = 3. pp, percentage points.

3.6 Exploratory Neurogenic Induction-Associated Morphology

Day-14 matched images showed process-bearing, neuron-like morphology in both groups, with more elongated and branched processes in the image from the 100 µM metformin-preconditioned group. The paired field-score median increased from 2.33 [IQR 2.17–2.33] to 3.00 [2.67–3.33] (HL shift +0.67 points; Holm $p = 0.008$) (Table 4; Fig. 6). This morphology-only result does not establish mature neuronal differentiation.

4. Discussion

The verified donor-level reanalysis showed a concentration-dependent pattern rather than a uniformly beneficial effect of metformin. The median XTT signal was highest at 100 µM. CFU-F/plating efficiency was higher at 100 µM and lower than control at 500 and 1000 µM after Holm adjustment. Interval PD showed a strongly ordered pattern across doses at every passage. However, no dose-specific PD contrast remained significant after adjustment across the full 12-comparison family. Osteogenic morphology did not differ statistically, whereas the neurogenic-associated field score was higher after 100 µM but remains exploratory.

The XTT findings should not be interpreted as proof of proliferation or universal safety. Lei et al. [7] reported concentration-dependent effects in human UC-MSCs, with lower concentrations supporting growth and 1000 µM pro-

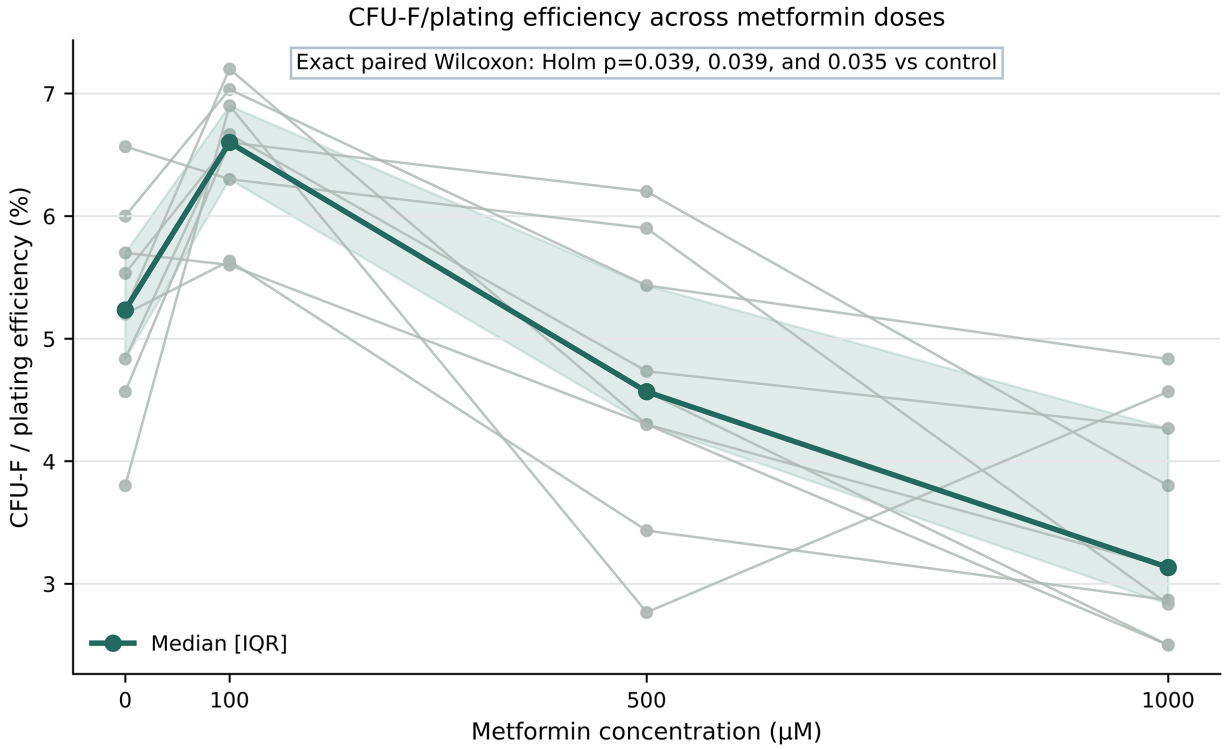

Fig. 3. Recalculated CFU-F/plating efficiency across metformin concentrations in nine eligible donors. Paired donor observations and the median summary are shown. Friedman χ^2 (3) = 19.99, $p < 0.001$; Kendall's W = 0.740. Exact paired Wilcoxon signed-rank control contrasts were Holm-adjusted (100 μM $p = 0.039$; 500 μM $p = 0.039$; 1000 μM $p = 0.035$).

Table 3. Count-derived interval PD and descriptive PDT by passage and metformin concentration.

Passage	Metformin (μM)	n	PD median [IQR]	PDT, h median [IQR]
P3	0	6	1.53 [1.33–1.56]	48.10 [43.35–54.87]
P3	100	6	1.57 [1.52–1.64]	46.54 [43.87–48.47]
P3	500	6	0.71 [0.62–0.79]	101.96 [87.11–120.23]
P3	1000	6 (PDT n = 5)	0.19 [0.07–0.33]	386.01 [210.32–405.23]
P4	0	6	1.19 [1.16–1.19]	63.37 [60.92–65.05]
P4	100	6	1.49 [1.45–1.53]	50.40 [49.51–52.24]
P4	500	6	1.01 [0.99–1.03]	74.85 [74.18–77.71]
P4	1000	6	0.81 [0.79–0.82]	97.39 [94.83–99.96]
P5	0	6	1.07 [1.06–1.10]	72.65 [69.35–76.15]
P5	100	6	1.40 [1.37–1.42]	56.13 [55.29–57.57]
P5	500	6	0.90 [0.87–0.91]	89.68 [87.13–91.89]
P5	1000	6	0.63 [0.62–0.65]	123.27 [122.49–131.47]
P6	0	6	0.96 [0.92–0.96]	86.17 [82.97–90.92]
P6	100	6	1.30 [1.28–1.34]	62.83 [62.63–63.23]
P6	500	6	0.75 [0.73–0.78]	111.54 [108.37–116.25]
P6	1000	6	0.52 [0.50–0.55]	157.85 [148.45–168.29]

PD, population doubling; PDT, population doubling time; IQR, interquartile range. PDT is descriptive and was not calculated for the P3/1000 μM net loss observation. All 12 dose-versus-control PD contrasts had a Holm-adjusted p-value of 0.375.

ducing inhibition. Bajetto et al. [14] observed progressively reduced growth at substantially higher, millimolar exposures in human UC-MSCs. Differences between those studies and the present 24-hour XTT experiment include cell preparation, dose, exposure time, culture medium, and outcome definition. Therefore, the modest XTT increase at 100 μM indicates greater tetrazolium-reduction activity under these conditions, not the absence of injury across all cellular domains.

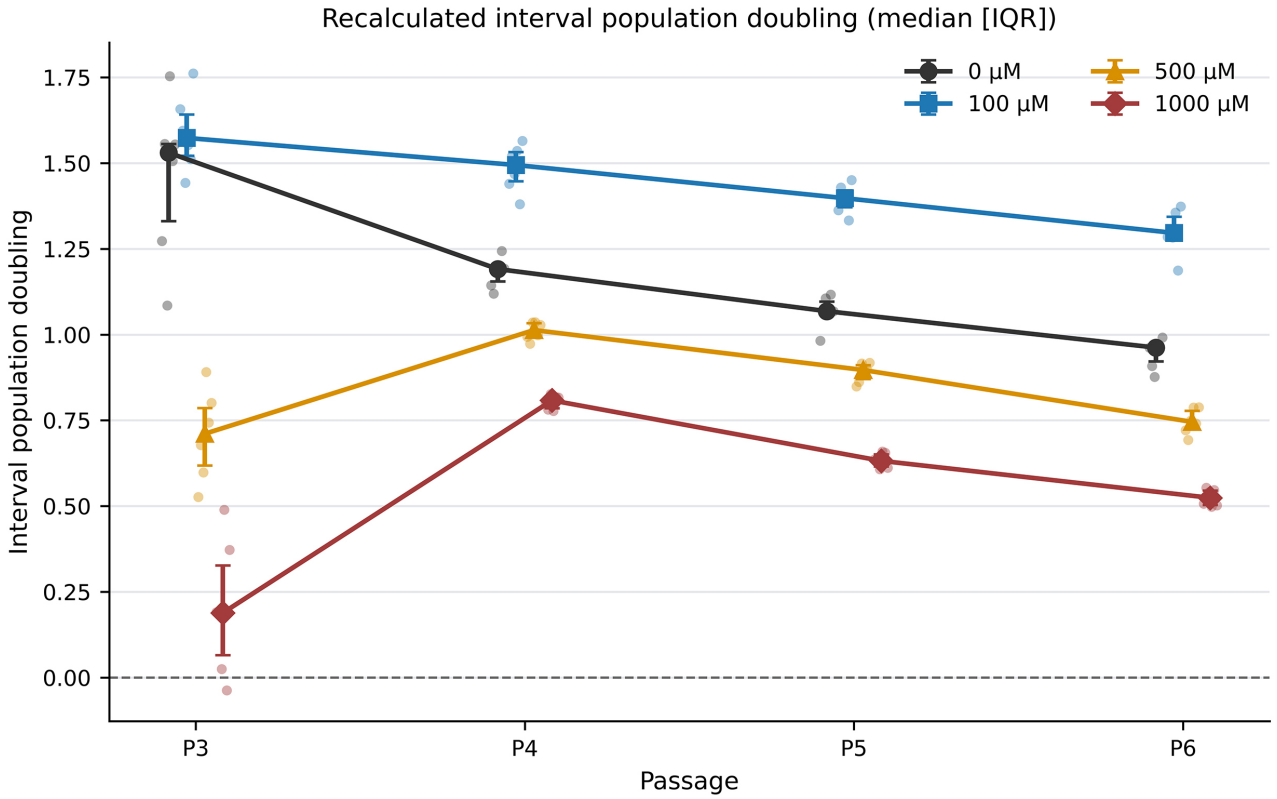

Fig. 4. Recalculated interval population doubling across P3–P6 in six complete donors without recorded overt contamination. Points show donor observations; symbols and lines show medians with IQR. Exact passage-specific Friedman tests remained significant after Holm adjustment, but none of the 12 exact paired Wilcoxon dose-versus-control contrasts remained significant (all Holm $p = 0.375$).

Table 4. Paired exploratory differentiation-associated morphology scores.

Assay	n	Control median [IQR]	100 µM median [IQR]	HL shift	Holm *p*
Osteogenic	9	2.67 [2.67–2.67]	2.67 [2.33–3.33]	+0.17	0.445
Neurogenic-associated	9	2.33 [2.17–2.33]	3.00 [2.67–3.33]	+0.67	0.008

Scores are arithmetic means of three 1–5 field scores per donor–condition and are exploratory. The neurogenic scores were based on day-14 assessments. Holm family size = 2. The neurogenic source header was inconsistent between days 7 and 14. HL, Hodges–Lehmann.

CFU-F/plating efficiency provided the clearest dose-specific evidence. Since exactly 1000 cells were seeded, the CFU-F and plating efficiency percentages are numerically identical and were reported once. The higher value at 100 µM suggests that a greater proportion of plated cells formed countable colonies, whereas 500 and 1000 µM were associated with fewer colonies. Selected studies in other stromal cell systems have linked metformin exposure to altered clonogenicity, senescence, or stemness, but the direction and magnitude of these effects vary by model and duration [15,16].

The count-derived PD data also favored 100 µM descriptively and showed lower values at 500 and 1000 µM, particularly in later passages. Nevertheless, the failed mixed-model stability check and non-significant fully adjusted dose-specific contrasts warrant caution. The data support an ordered within-donor passage pattern, but do not support a definitive claim that a particular dose improves long-term expansion. Reports that metformin can attenuate stress- or disease-associated senescence in other mesenchymal stromal cell models provide context but do not establish the same mechanism here [17,18].

Osteogenic cultures showed mineral-associated deposits on modified Von Kossa staining; however, the staining was qualitative, and the paired morphology score did not differ significantly. Published studies on UC-MSCs and perinatal stromal cells have reported metformin-associated osteogenic responses involving organic cation transport, phosphoinositide 3-kinase/protein kinase B/mechanistic target of rapamycin (PI3K/AKT/mTOR), or AMPK-related pathways [8,9,10]. Similar directional findings have been reported in bone marrow, adipose, and induced pluripotent stem cell-derived mesenchymal stromal models [19,20,21,22,23,24,25]. These studies support biologi-

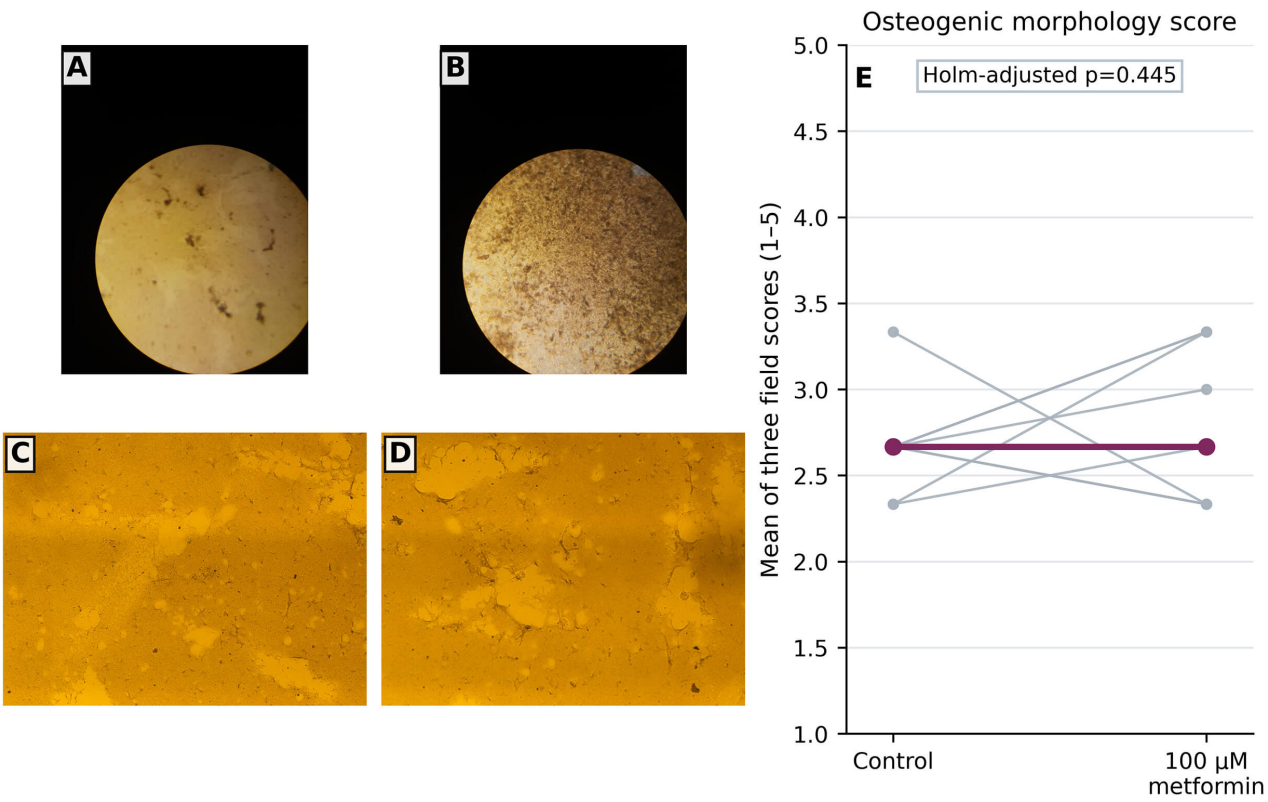

Fig. 5. Exploratory osteogenic morphology after 100 µM metformin preconditioning. (A) Representative day-14 control culture. (B) Representative day-14 culture preconditioned with 100 µM metformin. (C) Modified Von Kossa staining of the control culture. (D) Modified Von Kossa staining of the culture preconditioned with 100 µM metformin. Deposits were assessed qualitatively. (E) Paired donor field scores (n = 9). Grey points represent individual donor means calculated from three microscopic fields, and thin grey lines connect matched control and metformin-preconditioned observations from the same donor. The thick magenta line and large magenta points represent the group medians. No error bars are displayed; the corresponding interquartile ranges are reported in Table 4. Exact paired Wilcoxon signed-rank test with Holm adjustment, $p = 0.445$. No scale bars are provided because the original spatial-calibration metadata were unavailable. The images are presented solely as qualitative representative morphology and were not used for morphometric measurements.

cal plausibility; they do not convert the present qualitative staining into quantitative evidence of enhanced mineralization.

The neurogenic-associated result warrants even greater caution. The paired field score was higher after 100 µM preconditioning, and day-14 images showed more elongated, process-bearing cells. However, chemical induction can produce neuron-like morphology without demonstrating mature neuronal identity or function. Cai et al. [26] similarly reported neuron-like differentiation of gingival mesenchymal stromal cells in a metformin-containing scaffold, while acknowledging the limitations of claims of maturity. Neural precursor studies suggest a possible metformin-responsive neural context [11,27,28], but neural precursors and UC-MSCs are biologically distinct. Therefore, reviews recommend using multiple neuronal and glial markers, protein-level confirmation, and functional testing before claiming neuronal conversion [29].

A literature-based metabolic explanation is plausible but untested. Metformin can modulate mitochondrial complex I activity and cellular energy sensing [5], while AMPK and mTOR regulate metabolic homeostasis, autophagy, survival, and growth [30,31,32]. Moderate metabolic perturbation could yield a phenotype distinct from that of more severe energetic stress. In the absence of pathway assays, this framework remains a hypothesis and is not a demonstrated mechanism underlying the observed responses.

The principal strengths of this study are the use of independent donor-derived cultures, direct recalculation from available absorbance, dish-count, and seeded/harvested-cell records, and statistical methods that respect within-donor pairing. The dose screen and complementary endpoints, including metabolic, clonogenic, serial-expansion, and morphological assessments, also help distinguish a concentration window from an all-or-none drug effect.

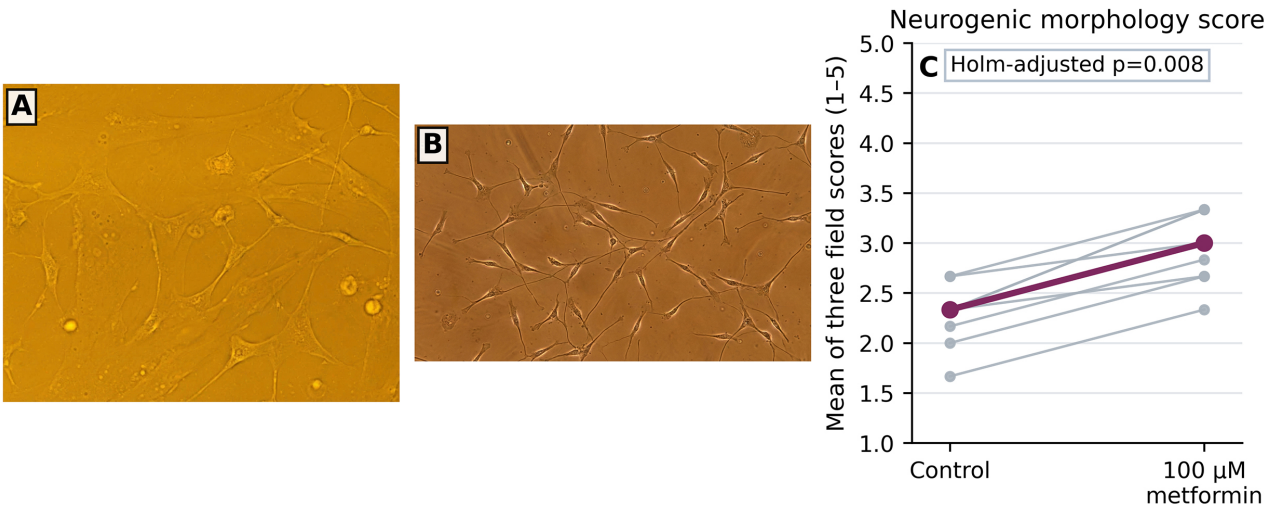

Fig. 6. Exploratory neurogenic induction-associated morphology. (A) Representative matched day-14 control culture. (B) Representative matched day-14 culture preconditioned with 100 µM metformin. (C) Paired donor field scores (n = 9). Grey points represent individual donor means calculated from three microscopic fields, and thin grey lines connect matched control and metformin-preconditioned observations from the same donor. The thick magenta line and large magenta points represent the group medians. No error bars are displayed; the corresponding interquartile ranges are reported in Table 4. Exact paired Wilcoxon signed-rank test with Holm adjustment, $p = 0.008$. The images show morphology only and do not establish mature neuronal identity. No scale bars are provided because the original spatial-calibration metadata were unavailable. The images were not used for morphometric measurements.

5. Limitations

This exploratory *in vitro* study has several limitations. Assay-specific sample sizes were small and not identical. Immunophenotypic characterization was qualitative, performed on an initial subset of early-passage cultures. Flow cytometry was not performed, and adipogenic and chondrogenic differentiation were not assessed; therefore, the cultures do not meet the minimum ISCT framework for complete quantitative and tri-lineage characterization. No specific mycoplasma detection assay was performed during or around the experimental period. The original and cryopreserved cultures are no longer available, making retrospective testing infeasible; consequently, the cultures are not described as having a laboratory-confirmed absence of mycoplasma. The available batch record also supported only a 1 mM metformin working treatment solution, not a fully documented primary-concentrate dilution history or a batch-specific certificate of analysis.

XTT reflects metabolic reduction and cannot establish proliferation or comprehensive toxicity. PD was analyzable in only six complete donors without recorded overt contamination; the planned mixed model was unstable; dose-specific contrasts were non-significant after full multiplicity adjustment; PDT was descriptive and undefined when PD was non-positive. Differentiation scores were unvalidated ordinal summaries; observer/blinding records were unavailable. Von Kossa staining was qualitative; calibration metadata for valid scale bars were unavailable; no additional neuronal/glial markers, protein-level assays, electrophysiology, quantitative mineralization, or direct AMPK/mTOR measurements were performed. Finally, qPCR findings were excluded because complete instrument exports, evidence of assay efficiency, and sample-level traceability were unavailable.

6. Conclusions

Metformin was associated with dose-dependent phenotypic responses in donor-derived UC-MSC cultures. The 100 µM condition produced the highest XTT metabolic signal and CFU-F/plating efficiency, whereas 500 and 1000 µM were associated with lower clonogenic and interval expansion measures. A higher neurogenic induction-associated morphology score at 100 µM was exploratory and does not establish mature neuronal differentiation. These findings support further dose-controlled investigation of metformin preconditioning but do not demonstrate a molecular mechanism, full MSC identity, or therapeutic efficacy.

Availability of Data and Materials

De-identified source records supporting the reportable analyses are available from the corresponding author on reasonable request, subject to institutional requirements.

Author Contributions

MJM and MMB designed the study; MJM, MMB, NY, and MS designed the methodology; MJM and AJG performed the investigation and laboratory work; MJM performed the formal analysis and data curation; MJM drafted the manuscript; MJM, MMB, NY, MS, and AJG reviewed

and edited the manuscript; MMB, NY, and MS supervised the project; MMB administered the project. All authors read and approved the final manuscript and agree to be accountable for all aspects of the work.

Ethics Approval and Consent to Participate

The study was approved by the Institutional Ethics Review Committee of King Edward Medical University, Lahore (No. 1030/RC/KEMU; 21 August 2019). This study was conducted in accordance with the Declaration of Helsinki. Umbilical cord tissue was collected after written maternal consent; collection followed routine delivery and did not alter obstetric care.

Acknowledgment

The authors thank the Advanced Research Centre of Biomedical Sciences, King Edward Medical University, Lahore, Pakistan, for technical and laboratory support.

Funding

This research received no external funding.

Conflicts of Interest

The authors declare no conflicts of interest.

Declaration of AI and AI-Assisted Technologies in the Writing Process

During preparation of this revised manuscript, OpenAI ChatGPT-5.6 Sol was used to assist with language editing, manuscript organization, preparation and checking of statistical-analysis code, and generation of revised data visualizations from author-supplied data. The authors reviewed and verified the resulting text, calculations, visualizations, and interpretations and take full responsibility for the final content.

References

[1] Rajput SN, Naeem BK, Ali A, Salim A, Khan I. Expansion of human umbilical cord derived mesenchymal stem cells in regenerative medicine. World Journal of Stem Cells. 2024; 16: 410–433. https://doi.org/10.4252/wjsc.v16.i4.410

[2] Dominici M, Le Blanc K, Mueller I, Slaper-Cortenbach I, Marini F, Krause D, et al. Minimal criteria for defining multipotent mesenchymal stromal cells. The International Society for Cellular Therapy position statement. Cytotherapy. 2006; 8: 315–317. https://doi.org/10.1080/14653240600855905

[3] Wilson AJ, Rand E, Webster AJ, Genever PG. Characterisation of mesenchymal stromal cells in clinical trial reports: analysis of published descriptors. Stem Cell Research & Therapy. 2021; 12: 360. https://doi.org/10.1186/s13287-021-02435-1

[4] Moll G, Ankrum JA, Olson SD, Nolta JA. Improved MSC Minimal Criteria to Maximize Patient Safety: A Call to Embrace Tissue Factor and Hemocompatibility Assessment of MSC Products. Stem Cells Translational Medicine. 2022; 11: 2–13. https://doi.org/10.1093/stcltm/szab005

[5] Foretz M, Guigas B, Viollet B. Metformin: update on mechanisms of action and repurposing potential. Nature Reviews. Endocrinology. 2023; 19: 460–476. https://doi.org/10.1038/s41574-023-00833-4

[6] Liu X, Li Z, Liu L, Zhang P, Wang Y, Ding G. Metformin-mediated effects on mesenchymal stem cells and mechanisms: proliferation, differentiation and aging. Frontiers in Pharmacology. 2024; 15: 1465697. https://doi.org/10.3389/fphar.2024.1465697

[7] Lei T, Deng S, Chen P, Xiao Z, Cai S, Hang Z, et al. Metformin enhances the osteogenesis and angiogenesis of human umbilical cord mesenchymal stem cells for tissue regeneration engineering. The International Journal of Biochemistry & Cell Biology. 2021; 141: 106086. https://doi.org/10.1016/j.biocel.2021.106086

[8] Al Jofi FE, Ma T, Guo D, Schneider MP, Shu Y, Xu HHK, et al. Functional organic cation transporters mediate osteogenic response to metformin in human umbilical cord mesenchymal stromal cells. Cytotherapy. 2018; 20: 650–659. https://doi.org/10.1016/j.jcyt.2018.02.369

[9] Shen M, Yu H, Jin Y, Mo J, Sui J, Qian X, et al. Metformin Facilitates Osteoblastic Differentiation and M2 Macrophage Polarization by PI3K/AKT/mTOR Pathway in Human Umbilical Cord Mesenchymal Stem Cells. Stem Cells International. 2022; 2022: 9498876. https://doi.org/10.1155/2022/9498876

[10] Manochantr S, Meesuk L, Chadee N, Suwanprateeb J, Tantrawatpan C, Kheolamai P. Improvement of osteogenic differentiation potential of placenta-derived mesenchymal stem cells by metformin via AMPK pathway activation. Stem Cell Research & Therapy. 2024; 15: 417. https://doi.org/10.1186/s13287-024-04014-6

[11] Xing C, Liu S, Wang L, Ma H, Zhou M, Zhong H, et al. Metformin enhances endogenous neural stem cells proliferation, neuronal differentiation, and inhibits ferroptosis through activating AMPK pathway after spinal cord injury. Journal of Translational Medicine. 2024; 22: 723. https://doi.org/10.1186/s12967-024-05436-9

[12] Roehm NW, Rodgers GH, Hatfield SM, Glasebrook AL. An improved colorimetric assay for cell proliferation and viability utilizing the tetrazolium salt XTT. Journal of Immunological Methods. 1991; 142: 257–265. https://doi.org/10.1016/0022-1759(91)90114-u

[13] Pochampally R. Colony forming unit assays for MSCs. Methods in Molecular Biology (Clifton, N.J.). 2008; 449: 83–91. https://doi.org/10.1007/978-1-60327-169-1_6

[14] Bajetto A, Pattarozzi A, Sirito R, Barbieri F, Florio T. Metformin potentiates immunosuppressant activity and adipogenic differentiation of human umbilical cord-mesenchymal stem cells. International Immunopharmacology. 2023; 124: 111078. https://doi.org/10.1016/j.intimp.2023.111078

[15] Acar MB, Ayaz-Güner Ş, Gunaydin Z, Karakukcu M, Peluso G, Di Bernardo G, et al. Proteomic and Biological Analysis of the Effects of Metformin Senomorphics on the Mesenchymal Stromal Cells. Frontiers in Bioengineering and Biotechnology. 2021; 9: 730813. https://doi.org/10.3389/fbioe.2021.730813

[16] Chinnapaka S, Yang KS, Flowers Q, Faisal M, Nerone WV, Rubin JP, et al. Metformin Improves Stemness of Human Adipose-Derived Stem Cells by Downmodulation of Mechanistic Target of Rapamycin (mTOR) and Extracellular Signal-Regulated Kinase (ERK) Signaling. Biomedicines. 2021; 9: 1782. https://doi.org/10.3390/biomedicines9121782

[17] Kim H, Yu MR, Lee H, Kwon SH, Jeon JS, Han DC, et al. Metformin inhibits chronic kidney disease-induced DNA damage and senescence of mesenchymal stem cells. Aging Cell. 2021; 20: e13317. https://doi.org/10.1111/acel.13317

[18] Le Pelletier L, Mantecon M, Gorwood J, Auclair M, Foresti R, Motterlini R, et al. Metformin alleviates stress-induced cellular senescence of aging human adipose stromal cells and the ensuing adipocyte dysfunction. elife. 2021; 10: e62635. https://doi.org/10.7554/eLife.62635

[19] Fan S, Zhang C, Sun X, Su C, Xue Y, Song X, et al. Metformin enhances osteogenic differentiation of BMSC by modulating macrophage M2 polarization. Scientific Reports. 2024; 14: 20267. https://doi.org/10.1038/s41598-024-71318-1

[20] Zhang M, Yang B, Peng S, Xiao J. Metformin Rescues the Impaired Osteogenesis Differentiation Ability of Rat Adipose-Derived Stem Cells in High Glucose by Activating Autophagy. Stem Cells and Development. 2021; 30: 1017–1027. https://doi.org/10.1089/scd.2021.0181

[21] Dong K, Zhou WJ, Liu ZH. Metformin enhances the osteogenic activity of rat bone marrow mesenchymal stem cells by inhibiting oxidative stress induced by diabetes mellitus: an *in vitro* and *in vivo* study. Journal of Periodontal & Implant Science. 2023; 53: 54–68. https://doi.org/10.5051/jpis.2106240312

[22] Wang P, Ma T, Guo D, Hu K, Shu Y, Xu HHK, et al. Metformin induces osteoblastic differentiation of human induced pluripotent stem cell-derived mesenchymal stem cells. Journal of Tissue Engineering and Regenerative Medicine. 2018; 12: 437–446. https://doi.org/10.1002/term.2470

[23] Ma J, Zhang ZL, Hu XT, Wang XT, Chen AM. Metformin promotes differentiation of human bone marrow derived mesenchymal stem cells into osteoblast via GSK3β inhibition. European Review for Medical and Pharmacological Sciences. 2018; 22: 7962–7968. https://doi.org/10.26355/eurrev_201811_16424

[24] Marycz K, Tomaszewski KA, Kornicka K, Henry BM, Wroński S, Tarasiuk J, et al. Metformin Decreases Reactive Oxygen Species, Enhances Osteogenic Properties of Adipose-Derived Multipotent Mesenchymal Stem Cells In Vitro, and Increases Bone Density In Vivo. Oxidative Medicine and Cellular Longevity. 2016; 2016: 9785890. https://doi.org/10.1155/2016/9785890

[25] Gao Y, Xue J, Li X, Jia Y, Hu J. Metformin regulates osteoblast and adipocyte differentiation of rat mesenchymal stem cells. The Journal of Pharmacy and Pharmacology. 2008; 60: 1695–1700. https://doi.org/10.1211/jpp.60/12.0017

[26] Cai S, Lei T, Bi W, Sun S, Deng S, Zhang X, et al. Chitosan Hydrogel Supplemented with Metformin Promotes Neuron-like Cell Differentiation of Gingival Mesenchymal Stem Cells. International Journal of Molecular Sciences. 2022; 23: 3276. https://doi.org/10.3390/ijms23063276

[27] Fatt M, Hsu K, He L, Wondisford F, Miller FD, Kaplan DR, et al. Metformin Acts on Two Different Molecular Pathways to Enhance Adult Neural Precursor Proliferation/Self-Renewal and Differentiation. Stem Cell Reports. 2015; 5: 988–995. https://doi.org/10.1016/j.stemcr.2015.10.014

[28] Wang J, Gallagher D, DeVito LM, Cancino GI, Tsui D, He L, et al. Metformin activates an atypical PKC-CBP pathway to promote neurogenesis and enhance spatial memory formation. Cell Stem Cell. 2012; 11: 23–35. https://doi.org/10.1016/j.stem.2012.03.016

[29] Neirinckx V, Coste C, Rogister B, Wislet-Gendebien S. Concise review: adult mesenchymal stem cells, adult neural crest stem cells, and therapy of neurological pathologies: a state of play. Stem Cells Translational Medicine. 2013; 2: 284–296. https://doi.org/10.5966/sctm.2012-0147

[30] Herzig S, Shaw RJ. AMPK: guardian of metabolism and mitochondrial homeostasis. Nature Reviews. Molecular Cell Biology. 2018; 19: 121–135. https://doi.org/10.1038/nrm.2017.95

[31] Kim J, Kundu M, Viollet B, Guan KL. AMPK and mTOR regulate autophagy through direct phosphorylation of Ulk1. Nature Cell Biology. 2011; 13: 132–141. https://doi.org/10.1038/ncb2152

[32] Panwar V, Singh A, Bhatt M, Tonk RK, Azizov S, Raza AS, et al. Multifaceted role of mTOR (mammalian target of rapamycin) signaling pathway in human health and disease. Signal Transduction and Targeted Therapy. 2023; 8: 375. https://doi.org/10.1038/s41392-023-01608-z